Research Article

Gold Supported on Metal Oxides for Carbon Monoxide Oxidation

Sonia A. C. Carabineiro[1] (✉), Nina Bogdanchikova[2], Miguel Avalos-Borja[2,†], Alexey Pestryakov[3], Pedro B. Tavares[4], and Jose L. Figueiredo[1]

[1] Laboratório de Catálise e Materiais, Associate Laboratory LSRE/LCM, Departamento de Engenharia Química, Faculdade de Engenharia, Universidade do Porto, 4200-465 Porto, Portugal

[2] Universidad Nacional Autónoma de México, Centro de Nanociencias y Nanotecnología, Carretera Tijuana-Ensenada, 22800, Ensenada, Baja California, México

[3] Tomsk Polytechnic University, 30, Lenin Avenue, Tomsk, 634050, Russia

[4] Universidade de Trás-os-Montes e Alto Douro, Centro de Química–Vila Real, Departamento de Química, 5001-911 Vila Real, Portugal

[†] On leave at Instituto Potosino de Investigación Científica y Tecnológica (IPICyT), San Luis Potosi, S.L.P., México

ABSTRACT

Au has been loaded (1% wt.) on different commercial oxide supports (CuO, La$_2$O$_3$, Y$_2$O$_3$, NiO) by three different methods: double impregnation (DIM), liquid-phase reductive deposition (LPRD), and ultrasonication (US). Samples were characterised by N$_2$ adsorption at −196 °C, high-resolution transmission electron microscopy, selected area electron diffraction, energy dispersive X-ray spectrometry, high-angle annular dark-field imaging (Z-contrast), X-ray diffraction, and temperature programmed reduction. CO oxidation was used as a test reaction to compare the catalytic activities. The best results were obtained with Au loaded by DIM on the NiO support, with an activity of 7.2×10^{-4} mol$_{CO} \cdot$g$_{Au}^{-1} \cdot$s^{-1} at room temperature. This is most likely related to the Au nanoparticle size being the smallest in this catalyst (average 4.8 nm), since it is well known that gold particle size determines the catalytic activity. Other samples, having larger Au particle sizes (in the 2–12 nm range, with average sizes ranging from 4.8 to 6.8 nm), showed lower activities. Nevertheless, all samples prepared by DIM had activities (from 1.1×10^{-4} to 7.2×10^{-4} mol$_{CO} \cdot$g$_{Au}^{-1} \cdot$s^{-1}, at room temperature) above those reported in the literature for gold on similar oxide supports. Therefore, this method gives better results than the most usual methods of deposition–precipitation or co-precipitation.

KEYWORDS

1. Introduction

The oxidation of CO to form CO$_2$ is the simplest and the most intensively studied reaction catalysed by gold [1–9]. Catalysts which promote this reaction at ambient temperatures find practical applications that include use in air-purification devices for indoor space, including gas masks, and for cleaning auto-motive exhaust gases. CO removal is also required in CO$_2$ lasers, and CO gas sensors are another application for gold catalysts.

Haruta and co-workers have intensively investigated

Address correspondence to sonia.carabineiro@fe.up.pt

the ability of gold to catalyse CO oxidation [1–5, 10, 11]. At the time of their early work in the 1980s, the activity for gold-supported catalysts came as a surprise [12, 13], but it is now well known that supported gold nano-catalysts are effective for CO oxidation at very low temperatures, being active even at –70 °C [6–9, 14, 15]. Activities do, however, depend on the choice of the metal oxide support. Although unsupported powdered gold (mean diameter 76 nm) is active for CO oxidation [16, 17], most of the studies made by Haruta and other groups have been on supported gold catalysts, with TiO_2, Fe_2O_3, and Al_2O_3 being the most common supports [6–9, 14, 18–23]. In this work, we wanted to use other metal oxides that have been employed to a lesser extent, namely, CuO, La_2O_3, NiO, and Y_2O_3.

The work of Tanielyan and Augustine [24], in which Au/CuO was prepared by co-precipitation (CP) under different conditions, is one of the few reports of the use of CuO as a support for CO oxidation gold catalysts. The most active catalysts were those which were heated in oxygen before use. Hutchings's group also prepared Au/CuO catalysts by CP [25, 26]. These materials were found to give sustained activity without deactivation during an 800 min experimental test [25]. Haruta used a CuO/Au composite film, prepared by the deposition of a thin CuO layer onto ultrafine Au particles for the optical detection of CO in air at around 250 °C [27]. CuO alone has also been rarely used as a catalyst for CO oxidation [28, 29].

Although it is considered an "active" support [19], NiO has been scarcely used for this reaction, when compared to other supports such as TiO_2 and Al_2O_3 [6–9, 15]. Haruta et al. prepared Au/NiO catalysts by CP which were very active for CO oxidation at tem-peratures as low as –70 °C [12, 30]. Behm's group also achieved good results for this type of catalyst using CP [19]. Dai and co-workers prepared highly active Au/NiO catalysts for CO oxidation using NiAu alloy nanoparticles [31]. The wet impregnation method has also been used by Radwan et al. who showed that addition of Au to NiO by this technique did not improve catalytic activity [32]. Other publications have also shown the good properties of Au/NiO catalysts [33–35]. In addition, NiO nanorings (without gold) showed an unexpected catalytic property for CO oxidation [36].

To the best of our knowledge, the only work reported in the literature on the use of Y_2O_3 as a support for gold is from Corma's group [37, 38]. In fact, this oxide, con-sidered an "inadequate" support for Au catalysts, was transformed into a highly active material when Au was deposited on nanocrystalline Y_2O_3 particles, instead of being prepared by a conventional precipitation method.

La_2O_3 is another example of a rarely used support. Au/La_2O_3 catalysts were obtained by precipitation techniques, and shown to be more active for CO oxidation when compared with Au/CeO_2 and Au/ZrO_2 prepared in the same way [39]. La_2O_3-supported Au(III) complexes synthesized from an $Au(CH_3)_2(C_5H_7O_2)$ [$C_5H_7O_2$ = acetylacetonate] precursor were also shown to be highly active and stable CO oxidation catalysts at room temperature, not suffering from deactivation even after 50 h of continuous operation in a flow reactor [40, 41]. The authors found that supported gold nanoparticles were readily oxidized by CO_2, suggesting that CO_2 could be the actual oxidant of gold in CO oxidation catalysis [41, 42].

As traditional deposition–precipitation (DP) [6–9, 15, 26, 43–45] and CP [6–9, 12, 13, 15, 19, 24–26, 29] are the most common methods to prepare oxide-supported gold catalysts, we wanted to combine the use of unusual supports with unusual methods, such as double impregnation (DIM) [46], and liquid-phase reductive deposition (LPRD) [47], in order to prepare Au nanoparticles. To the best of our knowledge, the only reports of the use of DIM are the work of Bowker et al. dealing with TiO_2 samples [46] and our previous work on CeO_2 [48, 49] and ZnO [50] catalysts. This method represents an environmentally and economically more favourable route to high activity gold catalyst production, when compared with the traditional DP method [46]. As far as we know, LPRD has only been used by Sunagawa et al. to prepare Pt and Au catalysts on Fe_2O_3, FeOOH, ZrO_2, and TiO_2 supports [47], and by us to prepare Au/CeO_2 [51] and Au/TiO_2 [52] catalysts. Ultrasonication (US) has only previously been used by our group to prepare highly active Au/ZnO materials [50]. In these methods, a washing procedure is carried out in order to eliminate residual chloride, which is well known to cause sintering of Au nanoparticles, thus rendering them inactive [6–9].

In this work, a comparison of the physicochemical properties of gold nanoparticles supported on different oxides (CuO, La_2O_3, NiO, and Y_2O_3), prepared by the methods described above (DIM, LPRD, and US), is presented. Samples were tested as catalysts for the oxidation of CO, which is a simple established model reaction to evaluate gold catalysts with many potential applications, but which is not yet fully understood, in spite of being intensively studied [6–9, 14]. A comparison is made with Au/CeO_2 and Au/TiO_2 catalysts also prepared by the DIM method.

2. Experimental

2.1 Oxide supports

The following commercial supports were tested: CuO (powder, purum, Riedel-de Haën), NiO (black, < 10 μm, Aldrich), La_2O_3 (99.99% metals basis, Aldrich), and Y_2O_3 (Art. 12412, Merck). These oxides were used both as received and after treatment at 400 °C in N_2 for 2 h (hereafter referred as "treated"). CeO_2 (Fluka) and TiO_2 P25 (Evonik Degussa) were also used for comparison.

2.2 Preparation of Au catalysts

Au was loaded on the oxide supports by DIM [46], LPRD [47], and US [50]. Briefly, DIM involves impregnating the support with an aqueous solution of the gold precursor and then with a solution of Na_2CO_3 [46, 48–50]. LPRD involves mixing a solution of $HAuCl_4$ with a solution of NaOH (with a ratio of 1:4 by mass) [47, 51, 52]. US involves dissolving the Au precursor in water and methanol, and sonicating for 8 h [50]. Further details can be found elsewhere [46–52].

2.3 Characterization techniques

The materials were analysed by adsorption of N_2 at –196 °C, in a Quantachrome NOVA 4200e apparatus. Temperature programmed reduction (TPR) and temperature programmed desorption (TPD) experiments were performed in a fully automated AMI-200 Catalyst Characterization Instrument (Altamira Instruments), equipped with a quadrupole mass spectrometer (Dymaxion 200 amu, Ametek). Further details can be found elsewhere [48, 49, 51, 53]. Conventional trans-

mission electron microscopy (TEM) measurements were performed with a JEOL 2010 microscope with a point-to-point resolution better than 0.19 nm. High resolution transmission electron microscopy (HRTEM), energy-dispersive X-ray spectroscopy (EDXS), and Z-contrast measurements were done on a FEI Tecnai F30 instrument. The Z-contrast images were collected using a high-angle annular dark-field detector (HAADF), in scanning transmission mode (STEM). The sample was mounted on a carbon polymer-supported copper micro-grid. A few droplets of a suspension of the ground catalyst in isopropyl alcohol were placed on the grid, followed by drying under ambient conditions. The average gold particle size and the particle size distribution were determined from measurements made on ~100–300 particles, depending on the sample. Simulations and fitting of selected area electron diffraction (SAED) patterns were carried out with the "JEMS" software [54]. X-ray diffraction (XRD) analysis was carried out in a PANalytical X'Pert MPD equipped with a X'Celerator detector and secondary monochromator (Cu $K\alpha$ λ = 0.154 nm, 50 kV, 40 mA; data recorded at a 0.017° step size, 100 s/step). Rietveld refinement with PowderCell software [55] was used to identify the crystallographic phases present and to calculate the crystallite size from the XRD diffraction patterns. Semi-quantitative estimation of gold loading was performed by EDXS. Further details can be found elsewhere [48–52].

2.4 Catalytic tests

Catalytic activity measurements were performed for CO oxidation, using a continuous-flow reactor. The catalyst sample (0.2 g) was placed on a quartz wool plug in a 45 cm long silica tube with 2.7 cm i.d., inserted into a vertical furnace equipped with a temperature controller. Feed gas (5% CO, 10% O_2 in He) was passed through the catalytic bed at a total flow rate of 50 $cm^3 \cdot min^{-1}$ (in contrast with most literature studies that use 1% CO or less [6–9, 15]). The composition of the outgoing gas stream was determined using a gas chromatograph equipped with a capillary column (Carboxen-1010 PLOT, Supelco) and a thermal conductivity detector. The activity results were obtained after the steady state was reached. Further details can be found elsewhere [48–52].

3. Results and discussion

3.1 Characterization of samples

3.1.1 Brunauer–Emmett–Teller (BET) surface area

Table 1 shows the characterisation results for the oxide supports obtained by N_2 adsorption at –196 °C. Thermal treatment lowered the BET surface area of NiO from 70 to 32 m^2/g. A decrease was also observed for CuO, but the surface areas are very small (5–11 m^2/g). The remaining oxides maintained their BET surface areas after the thermal treatment. The values are within those reported in literature for similar oxides of Cu and Ni [29, 30, 36]. Smaller values were obtained in this work for Y_2O_3 and La_2O_3 supports, when compared with the Ref. [37, 39–42, 56–58]. Addition of gold to the oxides, by any of the methods, did not produce significant changes in the BET surface areas, as seen in Table S-1 in the Electronic Supplementary Material (ESM).

3.1.2 XRD

Figure 1 shows the XRD results obtained for the oxide supports alone (as received), and loaded with 1% wt. Au by DIM. As can be seen in Fig. 1 and Table 1, the identified phases for the unloaded materials are the respective oxides, as expected, with the exception of La_2O_3 in which La(OH)$_3$ was found. This phase was also detected in the unsupported and supported La_2O_3 catalysts by other authors and is formed mostly by the hydrolysis of La_2O_3 during the exposure of the catalysts to atmospheric moisture [59]. In our study, this phase was also detected in the thermally treated sample, showing that thermal treatment at 400 °C for up to 24 h does not change the phase content.

The crystallite size of CuO is similar to that found by Radwan et al., with or without Au [32]. It is, however, much smaller than that found for another commercial CuO sample (Alfa Aesar: 115 nm) by Pillai and Deevi [29]. However, the same authors achieved smaller particle size (16 nm) by preparing a CuO sample by precipitation of copper nitrate [29].

The value for the commercial Y_2O_3 we used in this work (43 nm) is however, much larger than that found by Corma and co-workers for Y_2O_3 powder (27 nm) [37] and nanocrystalline Y_2O_3 (~6 nm) [37, 38]. The same is also true for the La_2O_3 we used (23 nm), compared
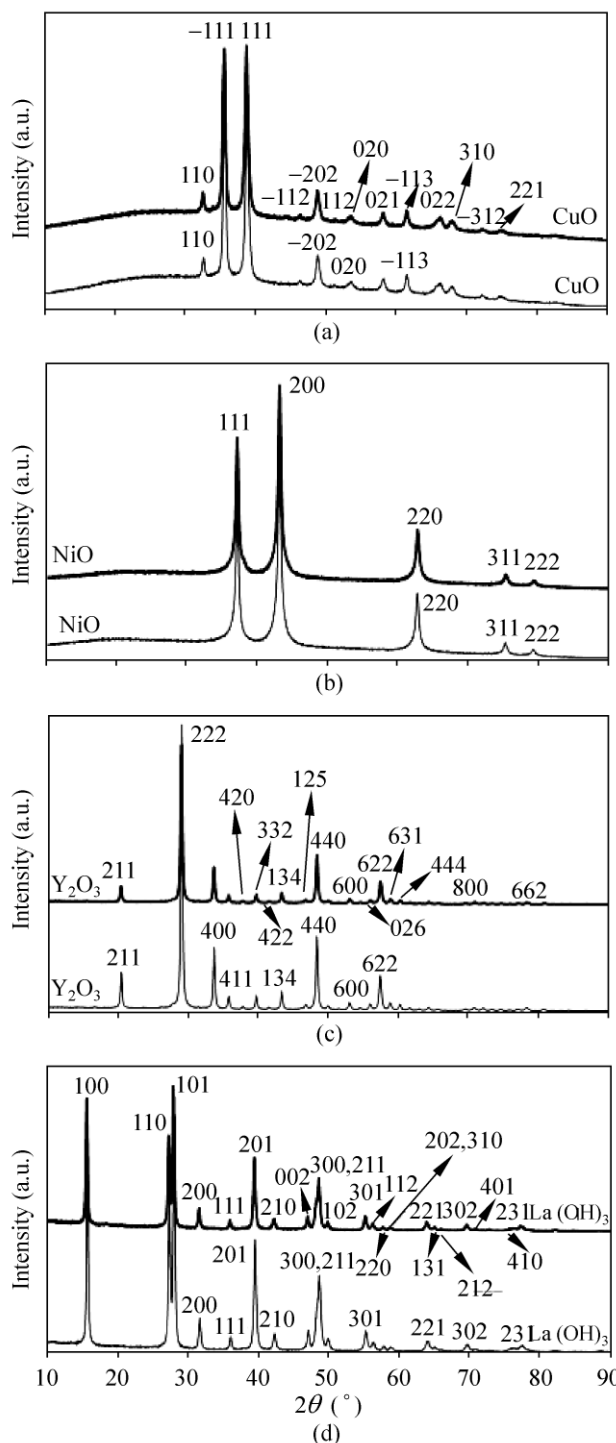

Figure 1 X-ray diffraction patterns of commercial CuO (a), NiO (b), Y_2O_3 (c), La_2O_3 (d), as received (lower pattern) and loaded with 1% wt. Au by DIM (upper pattern), with phases and respective crystal planes (Miller indexes) identified

with the literature value for La_2O_3 synthesized by base hydrolysis of lanthanum nitrate with NaOH in the presence of acetic acid (12 nm) [41].

Table 1 BET surface areas of the oxide samples obtained by adsorption of N_2 at −196 °C, crystallite sizes and phases detected by XRD

Metal oxide sample	BET area (m²/g)	Phase detected (crystal system, space group, reference code in database)	Crystallite size (nm)
CuO	11	CuO (monoclinic $C2/c$, 01-080-0076)	25
CuO (treated)	5	–	–
NiO	79	NiO (cubic Fm-$3m$, 00-047-1049)	26
NiO (treated)	32	–	–
Y_2O_3	9	Y_2O_3 (cubic, Ia-3, 01-083-0927)	43
Y_2O_3 (treated)	8	–	–
La_2O_3	11	La(OH)$_3$ (hexagonal, $P6_3/m$, 01-083-2034)	23
La_2O_3 (treated)[a]	10	La(OH)$_3$ (hexagonal, $P6_3/m$, 01-083-2034)	–

[a] Thermally treated for 24 h at 400 °C in N_2

The Au particle size could not be determined for any of the samples by XRD analysis, since the characteristic XRD reflection was absent in these materials. This is due to the low loading (1% wt.) and small size (as shown by HRTEM) of the Au particles present in these catalysts, and is consistent with the observations of other authors for Au/CuO catalysts [26].

3.1.3 HRTEM/HAADF/EDXS

Supports alone (untreated) and loaded with Au were analysed by HRTEM. Since the samples prepared by US were found to be less active for CO oxidation (see below), only samples prepared by DIM and LPRD were further characterised. EDXS confirmed the presence of gold (~1% wt. Au) for all samples.

Figure 2 shows images of the supports. It can be observed that the commercial CuO support (Fig. 2(a)) consists of a mixture of filament-like particles with average diameter of 20 nm and with lengths ranging from 20 to 150 nm. Larger round particle agglomerates of ~200 nm diameter are also present. The commercial sample of NiO (Fig. 2(b)) consists of a mixture of particles of several different sizes ranging from 5 to 100 nm. Interestingly, ~2.9% of "free carbon" was detected by EDXS (Fig. S-1 in the ESM), and thermo-gravimetry showed the presence of 2.5% carbon (Fig. S-2 in the ESM) in this material. Y_2O_3 (Fig. 2(c)) shows some interesting parallelepiped-like structures with sizes ranging from 10 to 90 nm. Finally, La_2O_3 (Fig. 2(d)) contains large agglomerates of particles ranging in size from ~300 to ~500 nm.
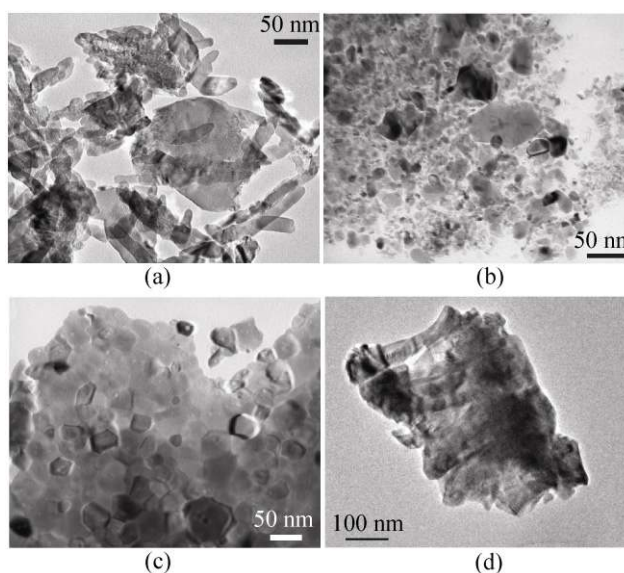

Figure 2 HRTEM images of the commercial supports: CuO (a), NiO (b), Y_2O_3 (c), and La_2O_3 (d)

HRTEM and HAADF results of supports loaded with Au are shown in Fig. 3. Gold particles are seen as darker spots in HRTEM and as bright dots in HAADF images. Figures 3(a) and 3(b) show representative HRTEM results for CuO with Au loaded by DIM and LPRD, respectively. Analysing the size distribution histogram of gold nanoparticles on this support (Figs. 4(a) and 4(b)), taken from several HRTEM images, it can be seen (Table 2) that although the gold size range for the two samples is the same (2–12 nm), the DIM sample has an average gold size which is smaller (5.8 nm) than the LPRD sample (6.6 nm). Larger Au particles were observed by Hutchings et al.
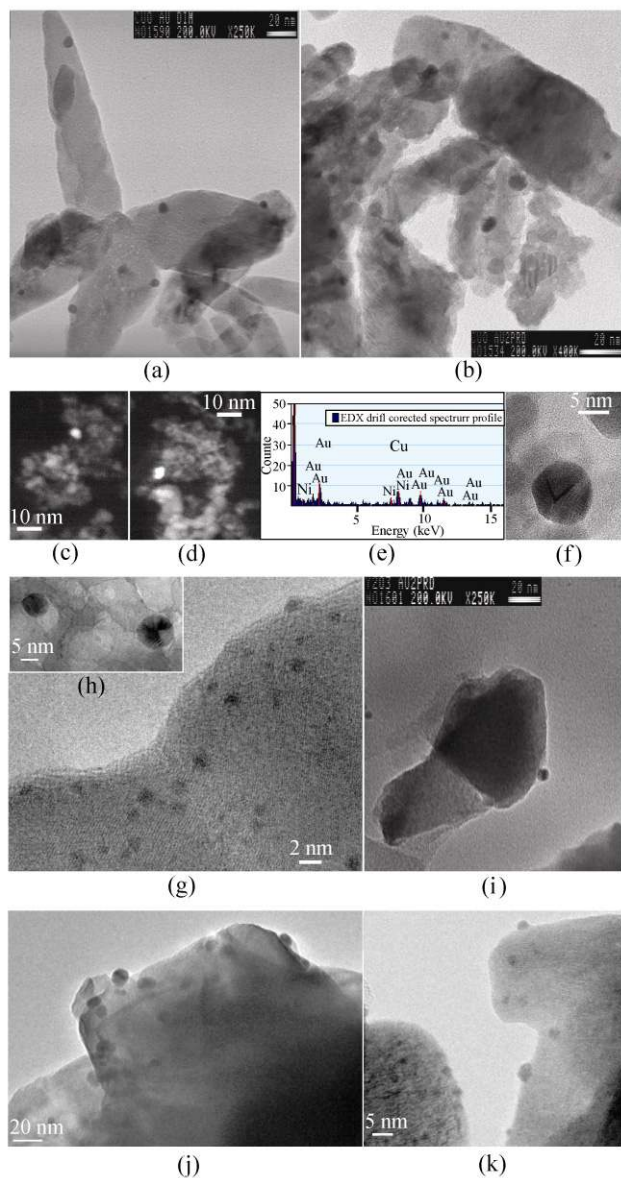
Au/oxide	Gold size range (nm)	Average gold particle size (nm)
Au/CuO (DIM)	2–12	5.8
Au/CuO (LPRD)	2–12	6.6
Au/NiO (DIM)	2–8	4.8
Au/NiO (LPRD)	2–11	5.4
Au/Y_2O_3 (DIM)	2–10	5.5
Au/Y_2O_3 (LPRD)	2–12	6.8
Au/La_2O_3 (DIM)	2–12	5.9
Au/La_2O_3 (LPRD)	2–12	6.1

Au/NiO samples were also analysed by HRTEM. In this case, however, the gold particles could not be identified, as the images look very similar to those obtained for the support alone (as seen in Figs. S-3 and S-4 in the ESM). This is due to the presence of free carbon on the support, as mentioned above (as seen in Figs. S-5 and S-6 in the ESM). Therefore HAADF was used in an attempt to image the gold particles. This technique is highly sensitive to variations in the atomic number of atoms in a sample, allowing Z-contrast images to be formed [48, 49, 51, 61]. In Figs. 3(c) and 3(d), gold particles supported on NiO prepared by DIM and LPRD, respectively, are seen as bright spots. Figure 3(e) shows an EDXS spectrum of one of the selected bright areas, confirming the presence of gold. When the sample was treated at 400 °C, some carbon was removed and gold particles were then easily seen by HRTEM (an example is shown in Fig. 3(f)). However, the treated samples were not as active for CO oxidation as the untreated ones, as will be discussed below. In addition, an attempt to synthesise NiO by an exotemplating method, similar to what was performed for CeO_2 [49] and MnO_2 [53] materials, was carried out. This sample, consisting of NiO prepared with a carbon template that was removed by calcination, was much less active than the commercial oxide, with or without Au. This means that the carbon found in commercial NiO must be related to its high activity. Further research is needed to clarify this point. The Au/NiO sample prepared by DIM in this work (with the commercial support) showed a narrower size distribution (2–8 nm) and a smaller average gold particle size of 4.8 nm (Fig. 4(c)
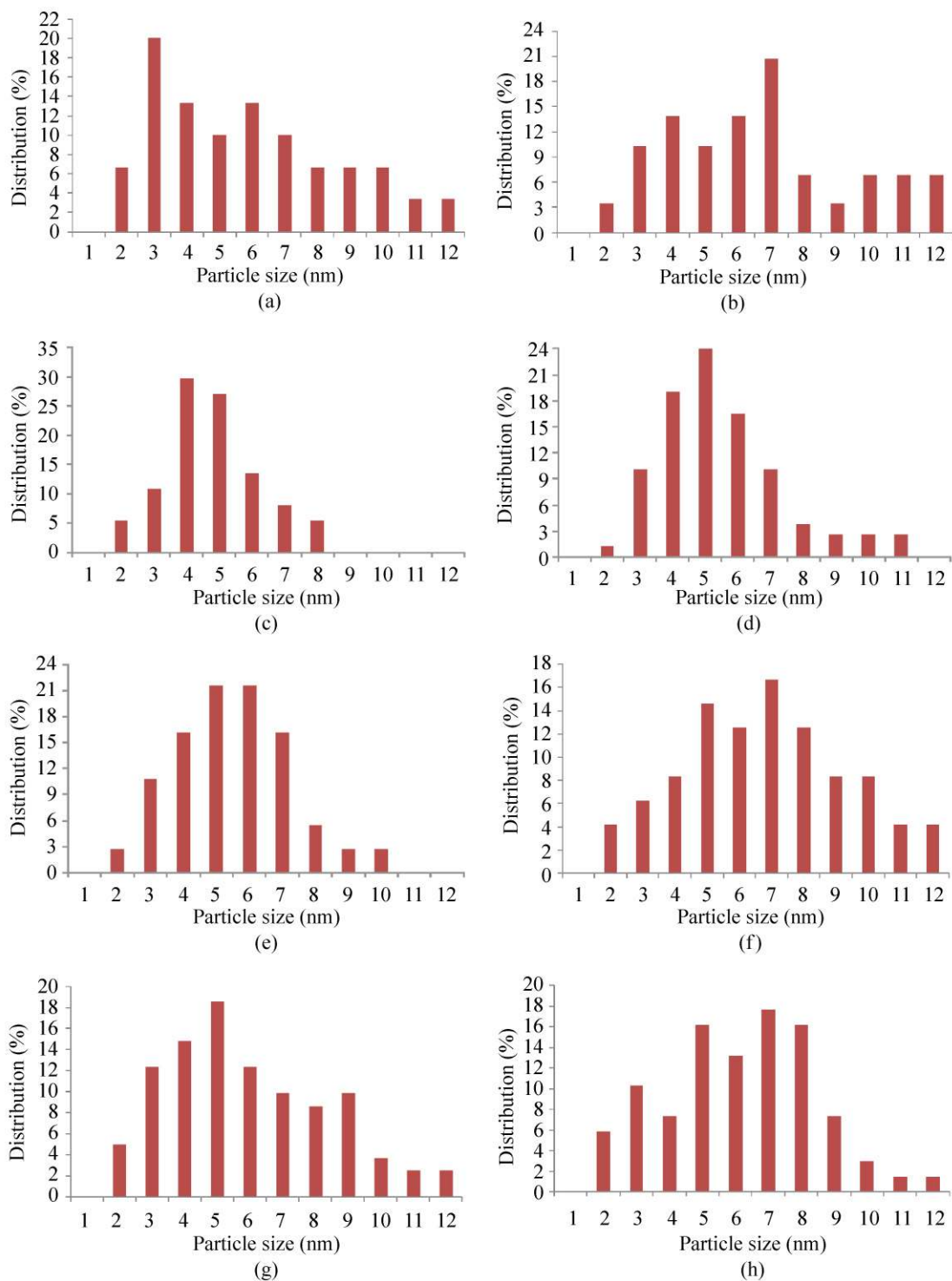
Figure 3 HRTEM images of CuO with Au loaded by DIM (a) and LPRD (b). HAADF images of NiO with Au loaded by DIM (c) and LPRD (d). EDXS spectrum (e) taken on a bright dot (gold particle) and HRTEM image of "treated" NiO with Au loaded by LPRD (f). HRTEM images of Y_2O_3 with Au loaded by DIM (g), showing a closer detail of Au nanoparticles as inset (h), and by LPRD (i). HRTEM images of La_2O_3 with Au loaded by DIM (j) and LPRD (k)

for Au/CuO catalysts prepared by CP, where the mean Au particle size was 20–30 nm, and there were many particles as large as 50 nm [25]. In contrast, Ko et al. obtained a Au/CuO sample prepared by DP from $Cu(OH)_2$ with an average gold particle size of 3.8 ± 0.5 nm [60].

Figure 4   Size distribution histograms of gold nanoparticles on CuO with Au loaded by DIM (a) and LPRD (b), NiO with Au loaded by DIM (c) and LPRD (d), Y_2O_3 with Au loaded by DIM (e) and LPRD (f), and La_2O_3 with Au loaded by DIM (g) and LPRD (h)

and Table 2), when compared to the LPRD material (Fig. 4(d) and Table 2). These are smaller than those found by Haruta et al. for Au/NiO catalysts prepared by CP and DP (~8 nm) [13, 62], but similar to the value of 3.2 ± 1 nm reported by Behm and co-workers using the same method [19].

The gold particles are clearly visible on the Y_2O_3 support. Figures 3(g) and 3(h) show the sample with Au loaded by DIM, in a general view and in closer detail, respectively. In Fig. 3(i), a detail of a piece of the support is seen with one gold particle on the right-hand side. The La_2O_3 support with Au loaded by DIM (Fig. 3(j)) and LPRD (Fig. 3(k)) also yielded nice HRTEM images. The histograms (Figs. 3(e)–3(h)) show that the size range varies from 2 to 12 nm (Table 2), as with the CuO samples. In general, the DIM method produced smaller particles for all materials.

Gold nanoparticles of smaller size (4 nm) were found by Guzman and Corma on nanocrystalline Y_2O_3 [37]. As for the literature concerning La_2O_3, a 2% wt. Au/La_2O_3 catalyst obtained by precipitation yielded a cluster size of 1–4 nm for the as-prepared catalyst [39]. However, sintering occurred at 800 °C, and the Au particle size increased, ranging between 20 and 40 nm [39]. Haruta and co-workers reported that gold nanoparticles smaller than 8 nm could be prepared on $La(OH)_3$ using CP [62].

3.1.4 SAED

Figure 5 shows the SAED images obtained for the untreated oxides with gold loaded by DIM. The simulations are shown for monoclinic CuO (Fig. 5(a)) and cubic Au (Fig. 5(b)) for the Au/CuO sample. Cubic NiO (Fig. 5(c)) and cubic Au (Fig. 5(d)) match well with the results for Au/NiO. Cubic Y_2O_3 (Fig. 5(e)) and cubic Au (Fig. 5(f)) were simulated for the Au/Y_2O_3 sample. The adjustment for cubic gold on Y_2O_3 (Fig. 5(f)) is not so clear; however the HRTEM and EDXS results showed the presence of gold. Finally, hexagonal $La(OH)_3$ (Fig. 5(g)) and cubic Au (Fig. 5(h)) were fitted for Au/La_2O_3. It was found that La_2O_3 did not adjust in this case. The results obtained match very well with those obtained by XRD (except that Au was not detected by this latter technique, as mentioned earlier).
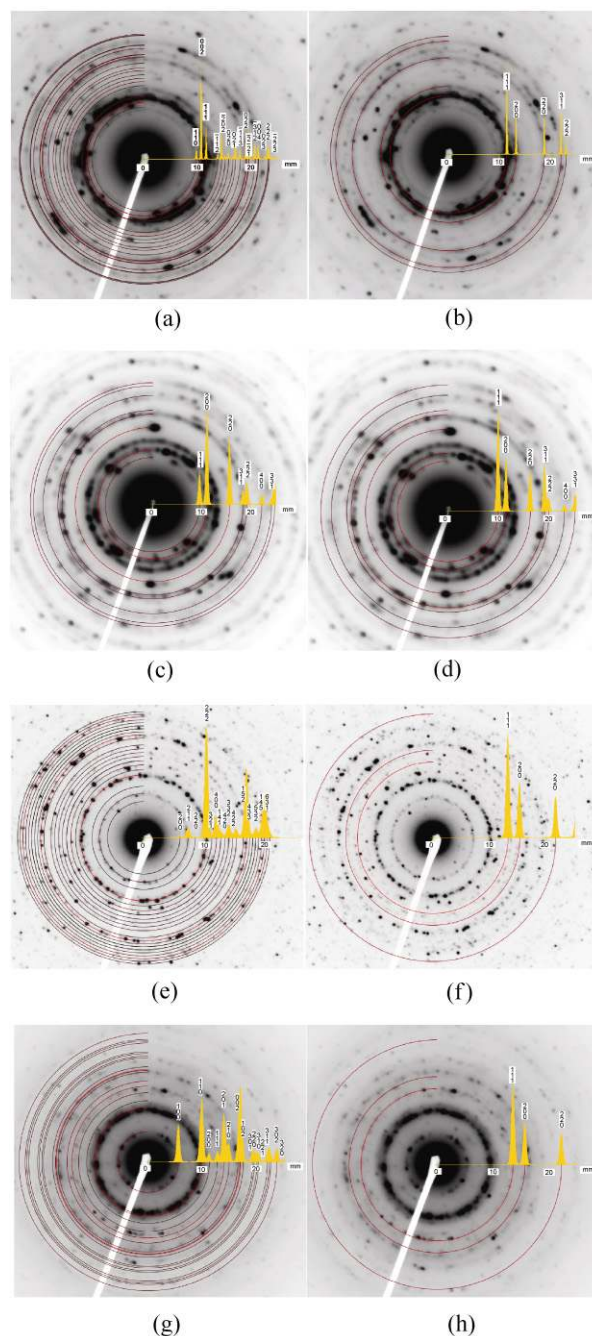

Figure 5 SAED images of CuO (a, b), NiO (c, d), Y_2O_3 (e, f), and La_2O_3 (g, h) with gold loaded by DIM. The images show the simulations for monoclinic CuO (a) and cubic Au (b) for Au/CuO sample; cubic NiO (c) and cubic Au (d) for Au/NiO; cubic Y_2O_3 (e), and cubic Au (f) for Au/ Y_2O_3; and hexagonal $La(OH)_3$ (g) and cubic Au (h) for Au/ La_2O_3

3.1.5 TPR

TPR results are shown in Figs. 6(a)–6(d), for the as-received commercial supports, and after loading with gold by DIM. One major peak is seen in the TPR

of the CuO sample at ~300 ℃, with a shoulder at ~244 ℃ (Fig. 6(a)). After the addition of gold, the peak temperatures decreased slightly to ~295 ℃ and ~238 ℃. According to the literature, two reduction peaks are expected for CuO, with or without Au, around ~200 ℃, which correspond to the CuO → Cu$_2$O and Cu$_2$O → Cu transitions [26].

Typical TPR spectra of NiO samples exhibit a main peak in the range 220–370 ℃ which is due to the Ni^{2+} → Ni^0 transition [63–66]. In our case (Fig. 6(b)), a major peak is observed at ~340 ℃, with a shoulder at ~250 ℃. After the addition of gold, these temperatures decreased to ~297 ℃ and ~215 ℃, respectively. Some authors have attributed the peak at lower temperature to non-stoichiometric surface oxygen and the other one to non-stoichiometric bulk oxygen in the oxide [65].

Figure 6(c) shows the TPR spectra of Y$_2$O$_3$, with and without Au. A very small peak is observed at ~500 ℃, in both cases. A small peak at ~630 ℃ has been reported by other authors for Y$_2$O$_3$ prepared from yttrium nitrate [67].

Negative TPR peaks were found for the La(OH)$_3$ (as noted above, lanthanum hydroxide was present instead of the expected oxide) materials as can be seen in Fig. 6(d), with or without gold, indicating no consumption of hydrogen. Again, water release was detected by mass spectrometry (MS), most likely meaning that La$_2$O$_3$ is being formed (La(OH)$_3$ → La$_2$O$_3$ + H$_2$O). In fact, a second TPR run produced the characteristic La$_2$O$_3$ trace, showing several small positive peaks, found in the literature for the oxide [39].

3.2 Catalytic tests

It was found that the activity for CO oxidation (with or without Au) of the thermally treated oxides did not improve when compared with the as-received samples; in fact, thermal treatment was detrimental in some cases. Therefore, only the results for the untreated samples are shown in Fig. 7. Before loading with Au, NiO, and CuO were the most active supports, achieving full conversion of CO at ~150 ℃, in contrast with results from previous authors reporting no conversion of CO for CuO at room temperature [26]. Figures 7(a) and 7(b) show that NiO was slightly more active than CuO at room temperature. In fact, other authors have shown that NiO nanorings exhibited unexpected catalytic
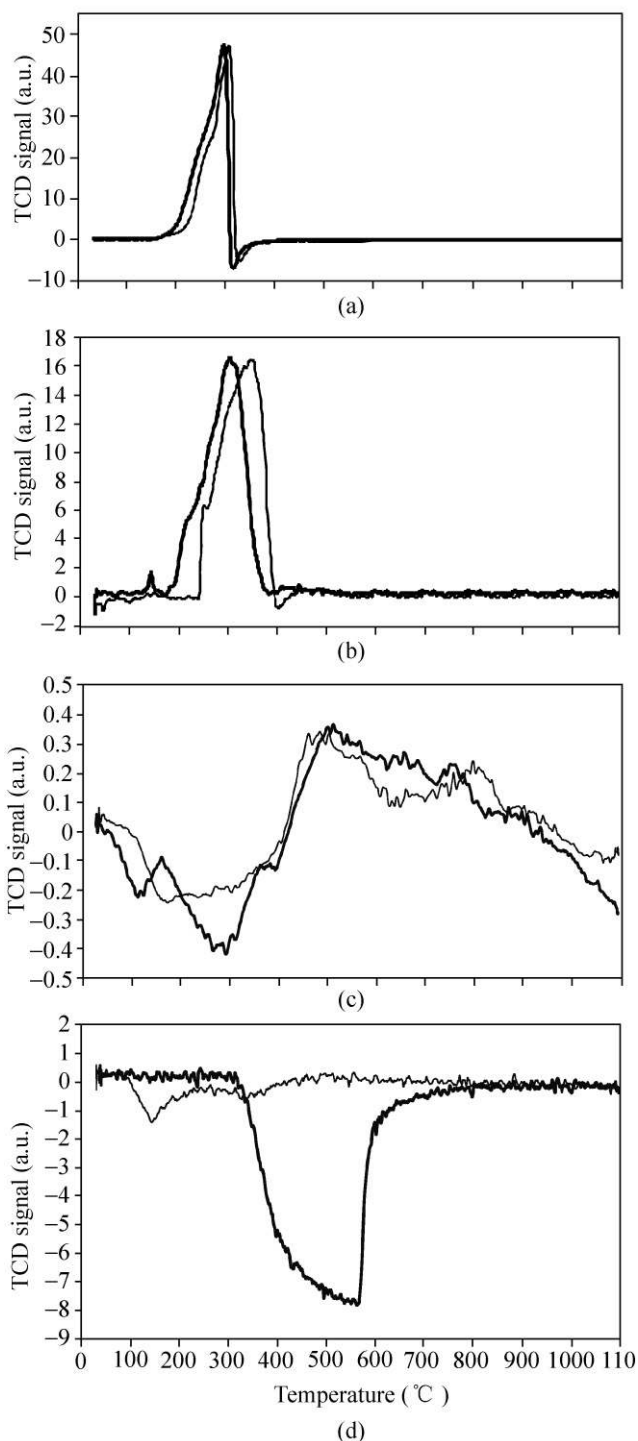

Figure 6 H$_2$-TPR profiles of the commercial CuO (a), NiO (b), Y$_2$O$_3$ (c), and La$_2$O$_3$ (d), as received (thin lines) and loaded with 1% wt. Au by DIM (thicker lines)

activity for CO oxidation [36]. The other supports (Figs. 7(c)–7(e)) only achieved full conversion of CO at ~650–700 ℃; however, Y$_2$O$_3$ had a better performance than La(OH)$_3$ between 200 ℃ and 600 ℃.
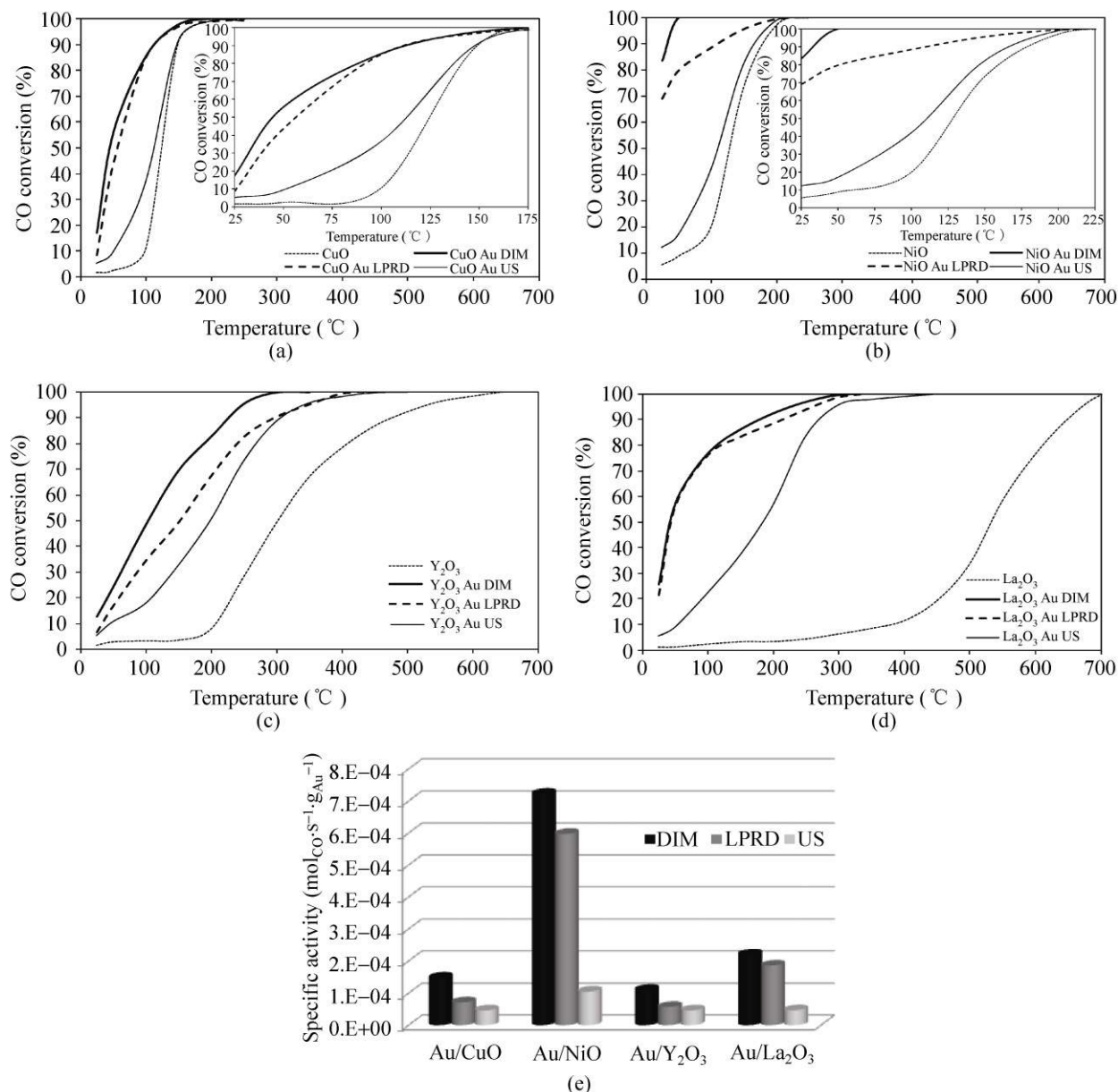
Figure 7 Plots of CO conversion (%) versus temperature for the CuO (a), NiO (b), Y_2O_3 (c), and La_2O_3 (d) supports alone and with Au loaded by different methods. Figures (a) and (b) have insets which show details at low temperature. Specific activities for the different Au/oxide catalysts determined at room temperature are shown in (e)

As expected, loading the samples with Au resulted in CO total conversion occurring at much lower temperatures than with the supports alone. DIM was found to be the best gold loading method. For CuO (Fig. 7(a)) and La_2O_3 (Fig. 7(e)), LPRD gave catalysts showing similar behaviour. For Y_2O_3 (Fig. 7(c)), the catalytic activity was similar for materials prepared by DIM and LPRD, but at higher temperatures DIM

gave materials with a better performance. For NiO, DIM is undoubtedly better than LPRD, with the catalyst achieving a conversion as high as 85% at room temperature, and full conversion at 50 °C; therefore, this sample is the most active found in this study. US was found to be the worst gold loading method for these supports, in contrast with the results found in our previous work with Au/ZnO catalysts [50].

Some gold catalysts described in the literature give full CO conversion at room temperature, but it has to be taken into account that most studies in the literature use 1% CO or less [6–9] (while we used 5% CO). In addition, most studies use higher loadings of Au [6–9] (while we used 1% wt.). Nevertheless, it is possible to see, in our case, that CO conversion at room temperature increased by up to 20 times on addition of gold (for the NiO and La_2O_3 with Au loaded by DIM), when compared to the unloaded samples.

The activities obtained at room temperature for our Au/CuO materials varied from 0.17 to 0.53 $mol_{CO} \cdot g_{Au}^{-1} \cdot h^{-1}$ (that is, 4.6×10^{-5} and 4.5×10^{-4} $mol_{CO} \cdot g_{Au}^{-1} \cdot s^{-1}$, as seen in Fig. 7(e), for the samples with Au loaded by US and DIM respectively), which is higher than the value reported by Solsona et al. at 25 °C for a Au/CuO catalyst prepared by CP (0.09 $mol_{CO} \cdot g_{Au}^{-1} \cdot h^{-1}$) [26].

Schubert et al. reported a value of 20×10^{-4} $mol_{CO} \cdot g_{Au}^{-1} \cdot s^{-1}$ at 80 °C for a Au/NiO catalyst prepared by CP [19]. This value cannot be compared with our DIM catalyst since it achieved full conversion at 50 °C (however, at room temperature, the value obtained was already 7.2×10^{-4} $mol_{CO} \cdot g_{Au}^{-1} \cdot s^{-1}$ as seen in Fig. 7(e)). Our other Au/NiO catalysts prepared by US and LPRD were less active, showing values of 3.6×10^{-4} $mol_{CO} \cdot g_{Au}^{-1} \cdot s^{-1}$ and 7.7×10^{-4} $mol_{CO} \cdot g_{Au}^{-1} \cdot s^{-1}$ at 80 °C, respectively (Fig. 7(e)).

Guzman and Corma [37] reported that the specific rate per gram of Au of a catalyst prepared with nanocrystalline Y_2O_3 was 2.1×10^{-4} $mol_{CO} \cdot g_{Au}^{-1} \cdot s^{-1}$ at 50 °C. Our Au/Y_2O_3 catalyst prepared by DIM showed an activity of 2.2×10^{-4} $mol_{CO} \cdot g_{Au}^{-1} \cdot s^{-1}$ at room temperature (Fig. 7(e)), which is a comparable value, especially considering that Guzman and Corma used nanocrystalline Y_2O_3, and that they obtained negligible activity for Au supported on a commercial Y_2O_3 material at the same temperature.

Russo et al. reported total CO conversion at ~225 °C (for 2% wt. Au supported on a La_2O_3 catalyst, using a mass of 800 mg and 2300 ppm CO) [39]. At that same temperature, our conversions were 90%–95% for the catalysts prepared by LPRD and DIM (Fig. 7(d)), which is remarkable, considering that our catalysts contained 1% wt. Au, and that we used a mass of 200 mg, and 5% CO in the feed.

In order to compare the results obtained with the DIM method for the supports used in this work with more common supports in literature, such as CeO_2 and TiO_2, additional CO oxidation tests were carried out for Au/CeO_2 and Au/TiO_2 samples prepared by DIM. The variation of CO conversion with temperature can be found in Figs. S-7 and S-8, respectively, in the ESM. The activity for Au on TiO_2 prepared by DIM was very low (in fact, negligible below 100 °C), when compared with that of the CuO, NiO, Y_2O_3, and La_2O_3 materials loaded with gold by the same method. Au/CeO_2 was more active than Au/TiO_2, achieving 38% CO conversion at low temperature [48], however Au/NiO DIM was still more active, since 85% conversion was found at room temperature, as discussed above.

4. Conclusions

1% wt. Au has been loaded on less commonly used commercial oxide supports (CuO, La_2O_3, Y_2O_3, NiO) by three different unusual methods: DIM, LPRD, and US.

Low BET surface areas were found for the oxide supports, as expected, which did not vary much after gold addition. Gold particle sizes from 2–12 nm were detected, with average sizes ranging from 4.8 to 6.8 nm.

The best results for CO oxidation were obtained for the NiO support with Au loaded by DIM, showing an activity of 7.2×10^{-4} $mol_{CO} \cdot g_{Au}^{-1} \cdot s^{-1}$ at room temperature. This is most likely related to it having the lowest Au nanoparticle size (an average of 4.8 nm), since it is well known that the Au particle size mostly determines catalytic activity. It was found that the commercial sample of NiO contained about 2.5% carbon, which prevented visualisation of gold particles by HRTEM, but they could be observed by HAADF. The removal of carbon by heating allowed the gold particles to be seen by HRTEM, but was detrimental to catalytic activity. Further research needs to be carried out on this subject.

Other samples, having larger Au particle sizes, showed lower activities for CO oxidation. Nevertheless, all samples prepared by DIM showed activities (from 1.1×10^{-4} to 7.2×10^{-4} $mol_{CO} \cdot g_{Au}^{-1} \cdot s^{-1}$, at room temperature) above those reported in the literature so far for gold on similar oxide supports. This shows that

this method (DIM) gives better results than the traditional methods like deposition–precipitation or co-precipitation.

Acknowledgements

Electronic Supplementary Material: Supplementary material (characterisation of oxide samples loaded with Au, EDXS, and thermogravimetry/differential scanning calorimetry (TG/DSC) results for the commercial NiO sample, HRTEM images of NiO with Au loaded by DIM and LPRD, CO conversion (%) versus temperature for the CeO_2 and TiO_2 commercial supports alone and with Au loaded by DIM) is available in the online version of this article at http://dx.doi.org/10.1007/s12274-010-0068-7.

References

[1] Haruta, M. Size- and support-dependency in the catalysis of gold. *Catal. Today* **1997**, *36*, 153–166.

[2] Haruta, M.; Date, M. Advances in the catalysis of Au nano-particles. *Appl. Catal. A: Gen.* **2001**, *222*, 427–437.

[3] Haruta, M. Catalysis of gold nanoparticles deposited on metal oxides. *Cattech* **2002**, *6*, 102–115.

[4] Haruta, A. When gold is not noble: Catalysis by nano-particles. *Chem. Rec.* **2003**, *3*, 75–87.

[5] Haruta, M. Gold as a novel catalyst in the 21st century: Preparation, working mechanism, and applications. *Gold. Bull.* **2004**, *37*, 27–36.

[6] Bond, G. C.; Thompson, D. T. Gold-catalysed oxidation of carbon monoxide. *Gold. Bull.* **2000**, *33*, 41–51.

[7] Bond, G. C.; Louis, C.; Thompson, D. T. *Catalysis by Gold*; Imperial College Press: London, United Kingdom, 2006.

[8] Carabineiro, S. A. C.; Thompson, D. T. Catalytic Applications for Gold Nanotechnology. In *Nanocatalysis*. Springer-Verlag: Berlin, Heidelberg, New York, 2007.

[9] Carabineiro, S. A. C.; Thompson, D. T. Gold Catalysis. In *Gold: Science and Applications*. CRC Press, Taylor and Francis Group: Boca Raton, London, New York, 2010.

[10] Hutchings, G. J.; Haruta, M. A golden age of catalysis: A perspective. *Appl. Catal. A: Gen.* **2005**, *291*, 2–5.

[11] Date, M.; Imai, H.; Tsubota, S.; Haruta, M. *In situ* measurements under flow condition of the CO oxidation over supported gold nanoparticles. *Catal. Today* **2007**, *122*, 222–225.

[12] Haruta, M.; Kobayashi, T.; Sano, H.; Yamada, N. Novel gold catalysts for the oxidation of carbon monoxide at a temperature far below 0-degrees-C. *Chem. Lett.* **1987**, 405–408.

[13] Haruta, M.; Yamada, N.; Kobayashi, T.; Iijima, S. Gold catalysts prepared by coprecipitation for low-temperature oxidation of hydrogen and of carbon monoxide. *J. Catal.* **1989**, *115*, 301–309.

[14] Hashmi, A. S. K.; Hutchings, G. J. Gold catalysis. *Angew. Chem. Int. Ed.* **2006**, *45*, 7896–7936.

[15] Aguilar-Guerrero, V.; Gates, B. C. Kinetics of CO oxidation catalyzed by supported gold: A tabular summary of the literature. *Catal. Lett.* **2009**, *130*, 108–120.

[16] Iizuka, Y.; Fujiki, H.; Yamauchi, N.; Chijiiwa, T.; Arai, S.; Tsubota, S.; Haruta, M. Adsorption of CO on gold supported on TiO_2. *Catal. Today* **1997**, *36*, 115–123.

[17] Iizuka, Y.; Tode, T.; Takao, T.; Yatsu, K. I.; Takeuchi, T.; Tsubota, S.; Haruta, M. A kinetic and adsorption study of CO oxidation over unsupported fine gold powder and over gold supported on titanium dioxide. *J. Catal.* **1999**, *187*, 50–58.

[18] Park, E. D.; Lee, J. S. Effects of pretreatment conditions on CO oxidation over supported Au catalysts. *J. Catal.* **1999**, *186*, 1–11.

[19] Schubert, M. M.; Hackenberg, S.; van Veen, A. C.; Muhler, M.; Plzak, V.; Behm, R. J. CO oxidation over supported gold catalysts-"inert" and "active" support materials and their role for the oxygen supply during reaction. *J. Catal.* **2001**, *197*, 113–122.

[20] Kung, H. H.; Kung, M. C.; Costello, C. K. Supported Au catalysts for low temperature CO oxidation. *J. Catal.* **2003**,

Springer

216, 425–432.

[21] Zhong, Z. Y.; Lin, J. Y.; Teh, S. P.; Teo, J.; Dautzenberg, F. M. A rapid and efficient method to deposit gold particles on catalyst supports and its application for CO oxidation at low temperatures. *Adv. Funct. Mater.* **2007**, *17*, 1402–1408.

[22] Perkas, N.; Zhong, Z.; Grinblat, J.; Gedanken, A. Deposition of gold particles on mesoporous catalyst supports by sono-chemical method, and their catalytic performance for CO oxidation. *Catal. Lett.* **2008**, *120*, 19–24.

[23] Zhu, Y. H.; Li, W.; Zhou, Y. X.; Lu, X. H.; Feng, X.; Yang, Z. H. Low-temperature CO oxidation of gold catalysts loaded on mesoporous TiO₂ whisker derived from potassium dititanate. *Catal. Lett.* **2009**, *127*, 406–410.

[24] Tanielyan, S. K.; Augustine, R. L. Effect of catalyst pretreatment on the oxidation of carbon-monoxide over coprecipitated gold catalysts. *Appl. Catal. A: Gen.* **1992**, *85*, 73–87.

[25] Hutchings, G. J.; Siddiqui, M. R. H.; Burrows, A.; Kiely, C. J.; Whyman, R. High-activity Au/CuO–ZnO catalysts for the oxidation of carbon monoxide at ambient temperature. *J. Chem Soc., Faraday Trans.* **1997**, *93*, 187–188.

[26] Solsona, B. E.; Garcia, T.; Jones, C.; Taylor, S. H.; Carley, A. F.; Hutchings, G. J. Supported gold catalysts for the total oxidation of alkanes and carbon monoxide. *Appl. Catal. A: Gen.* **2006**, *312*, 67–76.

[27] Ando, M.; Kobayashi, T.; Haruta, M. Combined effects of small gold particles on the optical gas sensing by transition metal oxide films. *Catal. Today* **1997**, *36*, 135–141.

[28] Avgouropoulos, G.; Papavasiliou, J.; Tabakova, T.; Idakiev, V.; Ioannides, T. A comparative study of ceria-supported gold and copper oxide catalysts for preferential CO oxidation reaction. *Chem. Eng. J.* **2006**, *124*, 41–45.

[29] Pillai, U. R.; Deevi, S. Room temperature oxidation of carbon monoxide over copper oxide catalyst. *Appl. Catal. B: Environ.* **2006**, *64*, 146–151.

[30] Haruta, M.; Yamada, N.; Kobayashi, T.; Iijima, S. Gold catalysts prepared by coprecipitation for low-temperature oxidation of hydrogen and carbon-monoxide. *J. Catal.* **1989**, *115*, 301–309.

[31] Zhou, S. H.; Yin, H. F.; Schwartz, V.; Wu, Z. L.; Mullins, D.; Eichhorn, B.; Overbury, S. H.; Dai, S. *In situ* phase separation of NiAu alloy nanoparticles for preparing highly active Au/NiO CO oxidation catalysts. *ChemPhysChem* **2008**, *9*, 2475–2479.

[32] Radwan, N. R. E.; Ei-Shall, M. S.; Hassan, H. M. A. Synthesis and characterization of nanoparticle CO₃O₄, CuO, and NiO catalysts prepared by physical and chemical methods to minimize air pollution. *Appl. Catal. A: Gen.* **2007**, *331*, 8–18.

[33] Zhang, W. X.; Tao, Y. G.; Jia, M. J.; Wu, T. H.; Li, X. M. Catalytic oxidation of CO at ambient temperature and humidity on Au/NiO prepared by using different methods. *Chem. J. Chin. Univ.* **1998**, *19*, 1317–1319.

[34] Wang, G. Y.; Zhang, W. X.; Jiang, D. Z.; Wu, T. H. CO oxidation over Au/MeOₓ at ambient temperature and humidity. *Acta Chim. Sinica* **2000**, *58*, 1557–1562.

[35] Wang, G. Y.; Zhang, W. X.; Cui, Y. C.; Lian, H. L.; Jiang, D. Z.; Wu, T. H. Effect of H₂O on catalytic performance of MOₓ, and Au/MOₓ catalysts for CO oxidation. *Chin. J. Catal.* **2001**, *22*, 408–410.

[36] Wang, D. S.; Xu, R.; Wang, X.; Li, Y. D. NiO nanorings and their unexpected catalytic property for CO oxidation. *Nanotechnol.* **2006**, *17*, 979–983.

[37] Guzman, J.; Corma, A. Nanocrystalline and mesostructured Y₂O₃ as supports for gold catalysts. *Chem. Commun.* **2005**, 743–745.

[38] Guzman, J.; Carrettin, S.; Fierro-Gonzalez, J. C.; Hao, Y. L.; Gates, B. C.; Corma, A. CO oxidation catalyzed by supported gold: Cooperation between gold and nanocrystalline rare-earth supports forms reactive surface superoxide and peroxide species. *Angew. Chem. Int. Ed.* **2005**, *44*, 4778–4781.

[39] Russo, N.; Fino, D.; Saracco, G.; Specchia, V. Supported gold catalysts for CO oxidation. *Catal. Today* **2006**, *117*, 214–219.

[40] Fierro-Gonzalez, J. C.; Bhirud, V. A.; Gates, B. C. A highly active catalyst for CO oxidation at 298 K: Mononuclear Au-III complexes anchored to La₂O₃ nanoparticles. *Chem. Commun.* **2005**, 5275–5277.

[41] Mihaylov, M.; Ivanova, E.; Hao, Y.; Hadjiivanov, K.; Knozinger, H.; Gates, B. C. Gold supported on La₂O₃: Structure and reactivity with CO₂ and implications for CO oxidation catalysis. *J. Phys. Chem. C* **2008**, *112*, 18973–18983.

[42] Mihaylov, M.; Ivanova, E.; Hao, Y.; Hadjiivanov, K.; Gates, B. C.; Knozinger, H. Oxidation by CO₂ of Au-0 species on La₂O₃-supported gold clusters. *Chem. Commun.* **2008**, 175–177.

[43] Grisel, R. J. H.; Nieuwenhuys, B. E. Selective oxidation of CO over supported Au catalysts. *J. Catal.* **2001**, *199*, 48–59.

[44] Gasior, M.; Grzybowska, B.; Samson, K.; Ruszel, A.; Haber, J. Oxidation of CO and C₃ hydrocarbons on gold dispersed on oxide supports. *Catal. Today* **2003**, *91–92*, 131–135.

[45] Szabo, E. G.; Hegedus, M.; Szegedi, A.; Sajo, I.; Margitfalvi, J. L. CO oxidation over Au/Al₂O₃ catalysts modified by MgO. *React. Kinet. Catal. Lett.* **2005**, *86*, 339–345.

[46] Bowker, M.; Nuhu, A.; Soares, J. High activity supported gold catalysts by incipient wetness impregnation. *Catal. Today* **2007**, *122*, 245–247.

[47] Sunagawa, Y.; Yamamoto, K.; Takahashi, H.; Muramatsu, A. Liquid-phase reductive deposition as a novel nano-particle synthesis method and its application to supported noble metal catalyst preparation. *Catal. Today* **2008**, *132*, 81–87.

[48] Carabineiro, S. A. C.; Silva, A. M. T.; Dražić, G.; Tavares, P. B.; Figueiredo, J. L. Gold nanoparticles on ceria supports for the oxidation of carbon monoxide. *Catal. Today* **2010**, *154*, 21–30.

[49] Carabineiro, S. A. C.; Bastos, S. S. T.; Órfão, J. J. M.; Pereira, M. F. R.; Delgado, J. J.; Figueiredo, J. L. Exotemplated ceria catalysts with gold for CO oxidation. *Appl. Catal. A: Gen.* **2010**, *381*, 150–160.

[50] Carabineiro, S. A. C.; Machado, B. F.; Bacsa, R. R.; Serp, P.; Dražić, G.; Faria, J. L.; Figueiredo, J. L. Catalytic performance of Au/ZnO nanocatalysts for CO oxidation. *J. Catal.* **2010**, *273*, 191–198.

[51] Carabineiro, S. A. C.; Silva, A. M. T.; Dražić, G.; Tavares, P. B.; Figueiredo, J. L. Effect of chloride on the sinterization of Au/CeO$_2$ catalysts. *Catal. Today* **2010**, *154*, 293–302.

[52] Santos, V. P.; Carabineiro, S. A. C.; Tavares, P. B.; Pereira, M. F. R.; Órfão, J. J. M.; Figueiredo, J. L. Oxidation of CO, ethanol, and toluene over TiO$_2$ supported noble metal catalysts. *Appl. Catal. B: Environ.* **2010**, *99*, 198–205.

[53] Carabineiro, S. A. C.; Bastos, S. S. T.; Orfao, J. J. M.; Pereira, M. F. R.; Delgado, J. J.; Figueiredo, J. L. Carbon monoxide oxidation catalysed by exotemplated manganese oxides. *Catal. Lett.* **2010**, *134*, 217–227.

[54] Available from: http://cimewww.epfl.ch/people/stadelmann/jemsWebSite/jems.html.

[55] Kraus, W.; Nolze, G. *PowderCell for Windows.* http://ccp14.minerals.csiro.au/ccp/web-mirrors/powdcell/av/v 1/powder/e cell.html.

[56] Margitfalvi, J. L.; Fasi, A.; Hegedus, M.; Lonyi, F.; Gobolos, S.; Bogdanchikova, N. Au/MgO catalysts modified with ascorbic acid for low temperature CO oxidation. *Catal. Today* **2002**, *72*, 157–169.

[57] Guzman, J.; Gates, B. C. Catalysis by supported gold: Correlation between catalytic activity for CO oxidation and oxidation states of gold. *J. Am Chem. Soc.* **2004**, *126*,

2672–2673.

[58] Szabo, E. G.; Tompos, A.; Hegedus, M.; Szegedi, A.; Margitfalvi, J. L. The influence of cooling atmosphere after reduction on the catalytic properties of Au/Al$_2$O$_3$ and Au/MgO catalysts in CO oxidation. *Appl. Catal. A: Gen.* **2007**, *320*, 114–121.

[59] Choudhary, V. R.; Mulla, S. A. R.; Uphade, B. S. Oxidative coupling of methane over supported La$_2$O$_3$ and La-promoted MgO catalysts: Influence of catalyst−support interactions. *Ind. Eng. Chem. Res.* **1997**, *36*, 2096–2100.

[60] Ko, E. Y.; Park, E. D.; Seo, K. W.; Lee, H. C.; Lee, D.; Kim, S. A comparative study of catalysts for the preferential CO oxidation in excess hydrogen. *Catal. Today* **2006**, *116*, 377–383.

[61] Carabineiro, S. A. C.; Silva, A. M. T.; Dražić, G.; Figueiredo, J. L. Analytical electron microscopy of gold nanoparticles on ceria, titania, and ceria-titania materials. In *Microscopy: Science, Technology, Applications and Education, Formatex Microscopy Book series*. Formatex Research Center, 2010.

[62] Sakurai, H.; Tsubota, S.; Haruta, M. Hydrogenation of CO over gold supported on metal oxides. *Appl. Catal. A: Gen.* **1993**, *102*, 125–136.

[63] Arena, F.; Frusteri, F.; Parmaliana, A.; Giordano, N. On the reduction of NiO forms in magnesia supported catalysts. *React. Kinet. Catal. Lett.* **1990**, *42*, 121−126.

[64] Parmaliana, A.; Arena, F.; Frusteri, F.; Giordano, N. Temperature-programmed reduction study of NiO–MgO interactions in magnesia-supported Ni catalysts and NiO–MgO physical mixture. *J. Chem Soc., Faraday Trans.* **1990**, *86*, 2663–2669.

[65] Kotsev, N. K.; Ilieva, L. I. Determination of nonstoichiometric oxygen in NiO by temperature-programmed reduction. *Catal. Lett.* **1993**, *18*, 173–176.

[66] Li, C. P.; Chen, Y. W. Temperature-programmed-reduction studies of nickel-oxide alumina catalysts—Effects of the preparation method. *Thermochim. Acta* **1995**, *256*, 457–465.

[67] Bellido, J. D. A.; Assaf, E. M. Effect of the Y$_2$O$_3$–ZrO$_2$ support composition on nickel catalyst evaluated in dry reforming of methane. *Appl. Catal. A: Gen.* **2009**, *352*, 179–187.